Grand canonical Monte Carlo simulations of the distribution and chemical shifts of xenon in the cages of zeolite NaA. II. Structure of the adsorbed fluid

Cynthia J. Jameson
Department of Chemistry, University of Illinois at Chicago, M/C 111, Chicago, Illinois 60607-7061

A. Keith Jameson
Department of Chemistry, Loyola University, Chicago, Illinois 60626

Hyung-Mi Lim and Bernoli I. Baello
Department of Chemistry, University of Illinois at Chicago, Chicago, Illinois 60607-7061

(Received 17 November 1993; accepted 30 December 1993)

The quantitative agreement between the results of a grand canonical Monte Carlo (GCMC) simulation and the various direct experimental measures of the distribution of the Xe atoms between adsorbed phase and gas phase, of intrazeolitic xenon among the alpha cages, and of the distribution of n Xe atoms in a Xe_n cluster within one alpha cage permit us to consider the structure of the adsorbed fluid in the GCMC simulation as a reasonable description of the actual structure. We provide here the adsorption sites for a single Xe atom in the alpha cage of zeolite NaA, the transition states between these adsorption sites, the one-body distribution functions for the individual clusters Xe_n inside the alpha cage, the Xe–Xe pair distribution functions for Xe_2 through Xe_8 at two temperatures, and some of the local minima in the configuration space of the clusters Xe_2 through Xe_8, i.e., some of the minimum energy configurations of the clusters.

I. INTRODUCTION

The physical insights obtained from measurements of properties of adsorbed molecules in porous solids such as adsorption isotherms, diffusion coefficients, isosteric heats of adsorption, and Henry's law constants, have been greatly enhanced by computer simulations of these systems.[1–24]

In the previous paper, we have found that grand canonical Monte Carlo (GCMC) simulations are able to successfully reproduce the directly measured distribution of Xe between zeolite and bulk gas phase (the adsorption isotherm) and the directly measured distribution of Xe atoms among the alpha cages for a very wide range of loadings: $\langle n\rangle = 0.45$ up to $\langle n\rangle = 6.73$ Xe atoms per cage at 296 and 360 K.[25] Even more significant is that the simulations also quantitatively reproduce the ^{129}Xe chemical shifts for the individual Xe_n clusters and their temperature dependences, which are indirect measures of the average distribution of the n Xe atoms within one alpha cage and how these distributions change with temperature. The ^{129}Xe chemical shift is very sensitive to the local environment of the Xe atom and it is most sensitive to the Xe–Xe internuclear separation.[26] With every one of the Xe atoms in the Xe_n cluster reporting the proximity of the other Xe atoms, the ^{129}Xe chemical shift is indeed a sensitive probe of the distribution of atoms within an alpha cage of the zeolite. The excellent detailed agreement between the simulated chemical shifts and the experimental spectra encourages us to examine the nature of the simulated distribution that leads to these observations. We examine here the minimum energy adsorption sites, the one-body distribution functions, and the pair distribution functions which provide a physical picture of the structure of the adsorbed fluid. We will show that the simulations lead to interesting physical insights regarding the nature of the adsorbed xenon in this zeolite.

II. RESULTS AND DISCUSSION

Details of the simulation are described in the preceding paper. Briefly, in modeling the xenon–zeolite interaction we used the sum of pairwise interactions between the Xe and the oxygen atoms and sodium ions located in the positions according to the refined x-ray structure of dehydrated zeolite NaA. The $Fm\bar{3}c$ symmetry of the unit cell and the coordinates of the unique atoms were obtained from Pluth and Smith.[27] A phase transition which takes the crystal lattice from $Fm\bar{3}c$ to rhombohedral $R\bar{3}c$ at 355 K is known to exist.[28] In the simulations the lattice is taken to be rigid, in the $Fm\bar{3}c$ space group and perfectly crystalline. The Xe–O and Xe–Na^+ interactions were described by Lennard-Jones functions that were taken from the set used by Woods and Rowlinson in their simulations of Xe in zeolites NaX and NaY.[29] Periodic boundary conditions with the minimum image convention was used. Consistent with this, the potential functions were cut-and-shifted with a cutoff at half the lattice parameter. The Xe–Xe interactions are likewise taken to be pairwise additive with a potential function of the Maitland–Smith form[30] fit to the best available Xe–Xe gas two-body potential of Aziz and Slaman, which reproduces all the available xenon experimental data: scattering and thermophysical properties, as well as spectroscopic data including the vibrational spectra of the dimer.[31] This too was cut and shifted as were the shielding functions that are based on *ab initio* calculations of nuclear shielding in model systems.[32] Shielding was also taken to be pairwise additive and only the isotropic part of the shielding tensor was considered in the simulation of the isotropic chemical shifts. Although the *ab initio* cal-

 0021-9606/94/100(8)/5977/11/$6.00

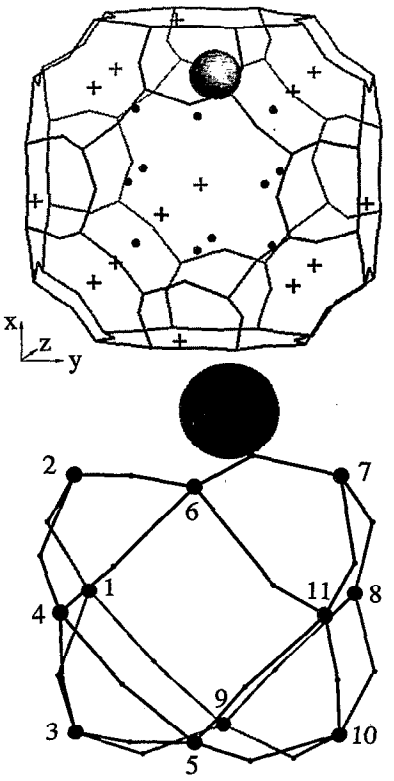

FIG. 1. Adsorption sites and transition states for a single Xe atom in the alpha cage of zeolite NaA. The top figure shows the adsorption sites; the origin is at the center of a beta cage. The lower figure is exactly the same view of the adsorption sites, magnified and labeled in numerical order according to increasing energy. The transition states are also shown, connected to the minimum energy sites by straight lines (not reaction paths).

culations provide the full tensor, only the isotropic part determines the NMR peak positions in these systems at the temperatures of the experiments. The simulations were carried out in the grand canonical Monte Carlo (GCMC) scheme using the Norman–Filinov method of constructing the Markov chain, following the work of Woods and Rowlinson.[1,2,33] The chemical potential and the temperature were parameters that were fixed and the numbers of particles were allowed to fluctuate. Initial configurations were prepared and the system allowed to equilibrate in 10^5 cycles, consisting of one displacement step followed by two create or annihilate steps. These results were discarded and followed by data collecting 10^6 cycles. During the data-collecting phase, one-body distributions, Xe–Xe pair distributions, shieldings of Xe in clusters (cages containing a particular number of Xe atoms), and other statistics were collected. Simulation temperatures were between 180 and 520 K and chemical potentials were set so as to have equilibrium occupancies of from 1 up to 60 Xe atoms per unit cell. The results which could be compared directly with experiment are presented in the preceding paper. Here we provide the results which describe the structure of the adsorbed fluid, which in fact determines the agreement between simulated properties and experimental properties such as average chemical shifts of the Xe that are in cages containing exactly five Xe atoms, e.g., or the fractions of alpha cages containing none up to eight Xe atoms at some average occupancy and temperature. On the other hand, the excellent agreement between the very detailed experimental information and the simulations do not guarantee that the description of the structure of the adsorbed fluid which produced such excellent reproduction of experiment is correct or even unique. Nevertheless, since there has never been as detailed a match with as many independent pieces of information as we have demonstrated in the preceding paper, we are encouraged to offer up the description of the structure of this adsorbed fluid.

A. The adsorption sites and transition states for a single Xe atom

We found 11 minimum energy sites in the alpha cage for a single Xe atom, which we show in Fig. 1 as dark spots marking their locations within the alpha cage framework. The origin is at the center of a beta cage, the axes oriented as shown in the figure. The dimension of the alpha cage shown is half of the lattice parameter (12.2775 Å). The lower part of the figure shows the adsorption sites in exactly the same view, magnified and labeled. The framework has a high degree of symmetry, and so a high degree of symmetry is also observed in the structure of the adsorbed fluid. In the dehy-

TABLE I. Low-energy transition states between the 11 adsorption sites of a single Xe in an alpha cage. All energies are relative to the lowest-energy adsorption site, in J/mol. Locations of sites are shown in Fig. 1 and the relative energies are shown (along the diagonal) in the table below, with the transition state energies.

Adsorption site	1	2	3	4	5	6	7	8	9	10	11
1	0.										
2	1200.7	16.2									
3	2229.2	*x*	73.3								
4	*x*	1901.9	3837.9	73.5							
5	*x*	*x*	3837.	3837.	82.5						
6	*x*	3882.5	*x*	2220.7	*x*	177.7					
7	*x*	*x*	*x*	*x*	*x*	1901.1	180.6				
8	*x*	*x*	*x*	*x*	*x*	*x*	1571.3	180.7			
9	3883.4	*x*	1891.2	*x*	*x*	*x*	*x*	2241.1	193.6		
10	*x*	*x*	*x*	*x*	2255.2	*x*	*x*	2024.	1651.4	246.7	
11	*x*	*x*	*x*	*x*	1929.1	1377.6	2350.9	*x*	*x*	4018.2	262

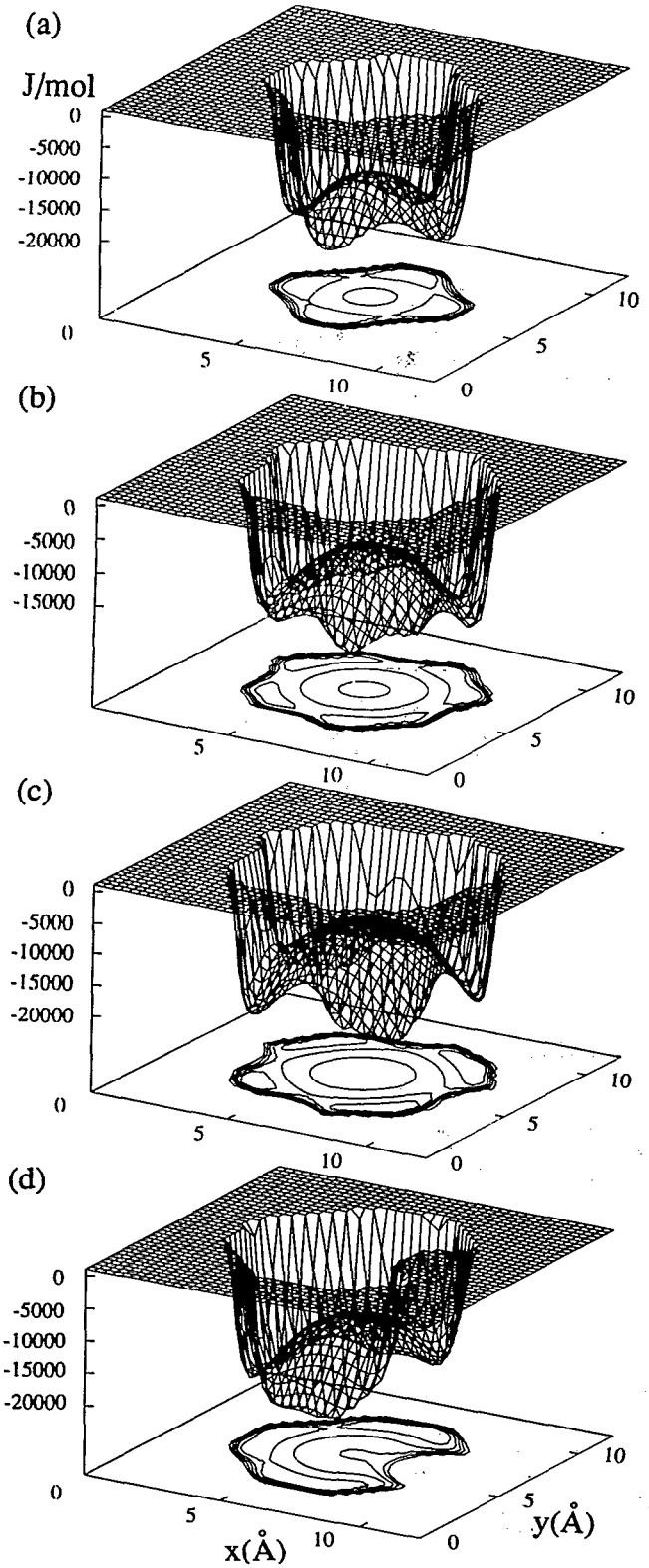

FIG. 2. Potential energy surface for the interaction of a single Xe atom with the zeolite NaA. The origin is at the center of a beta cage and the slices shown are for (a) $z=3.7365$ Å; (b) $z=4.982$ Å; (c) $z=6.2275$ Å; (d) $z=7.473$ Å. The asymmetry in picture (d) is due to the location of Na(III).

drated zeolite NaA ($Fm\bar{3}c$ symmetry) one-eighth of the unit cell has the formula $Na_8Al_{12}Si_{12}O_{24}$. The three cation sites (labeled I, II, and III) have been determined by x-ray structure refinement.[27] Eight Na^+ ions are associated with the six-oxygen rings (site I) and three are located off-center in the six eight-ring windows (site II) shared with neighboring cages. The one Na(III) ion, which (at 9.675, 6.139, and 9.675 Å) is coordinated to a four ring in a one-sided square pyramidal arrangement, occupies significant space roughly where the 12th minimum energy site would have been. The Na(III) is shown here as a sphere located at the coordinates from the x-ray structure.[27] For clarity the Na(II) ions are represented as + signs only and the Si, O, and Al atoms in the framework are represented by vertices interconnected by lines representing bonds. The adsorption sites have very similar energies, all within 262 J/mol of each other. The minimum energy sites are numbered 1 to 11 in order of increasing energy. Their relative energies are given in Table I. The multidimensional potential energy surface (PES) constructed in the preceding paper[25] is represented in Fig. 2 by selected slices at $z=3.7365$, 4.982, 6.2275, and 7.473 Å.

We have determined the transition states connecting the 11 adsorption sites by using a grid search through the 40 $\times 40 \times 40$ array representation of the potential surface for a single Xe atom in an alpha cage, as well as by using the method of Cerjan and Miller.[34] The first method allows an examination of the terrain (on the potential energy surface in the regions between one adsorption site and another), as an imaginary plane sweeps along the x axis, in small increments of x, e.g., the lowest-energy point on the plane is easily recognized and the trajectory connecting these lowest-energy points from one imaginary plane to the next provides the trace along the bottom of the valley. In doing this we find the saddle points. In this particular case, we used a rather coarse grid so this method provides only the coarse coordinates for the transition states (0.306 94 Å resolution). The method of Cerjan and Miller provides a stable algorithm for "walking uphill" from a minimum on the potential surface to a transition state. This algorithm also provides a much more efficient and accurate procedure for following the reaction path from a transition state down to a minimum than by simply following the gradient vector itself. All the saddles reported here (Fig. 1 and Table I) are true transition states with exactly one negative eigenvalue of the Hessian matrix. Each transition state found by this technique was further verified by steepest descent to the minimum energy adsorption sites. Figure 1 provides a view of the number and locations of the adsorption sites and the low-energy transition states connecting them. The coordinates of the adsorption sites and the transition states are shown and straight lines (not the reaction paths) connect the adsorption sites and transition states. These are only the lowest-energy transition states connecting the adsorption sites. There are numerous other higher-energy transition states between these sites. It is quite clear from the potential energy surfaces shown in Fig. 2 that the low-energy paths must lie close to the walls of the cavity. Starting from the locations of the 11 adsorption sites, there are 20 such obvious connections along the walls. Figure 1 shows these connections which are indeed the same ones that involve the

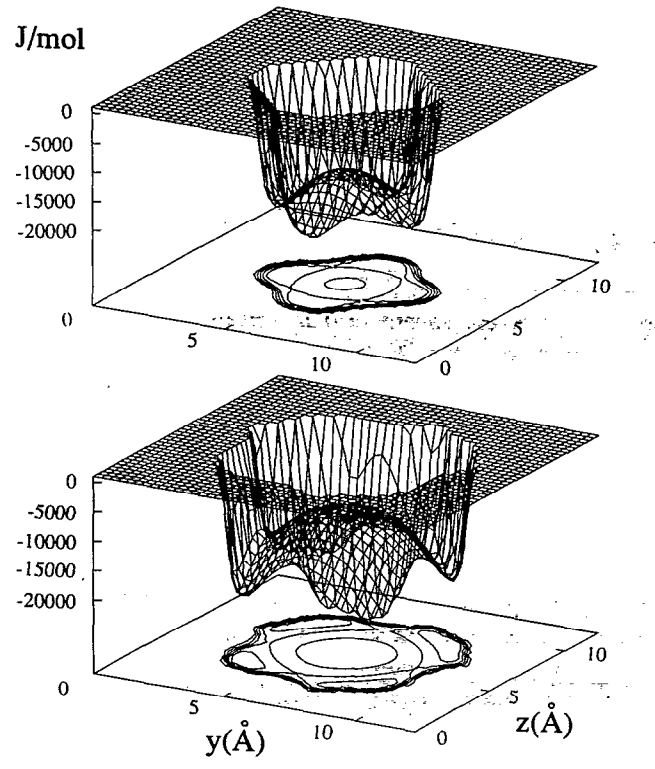

FIG. 3. The $x=3.6$ Å slice (top figure) of the potential energy surface for one Xe atom in the alpha cage of zeolite NaA, showing sites 3, 5, 10, and 9, contrasted with the $x=6.15$ Å slice (bottom figure) containing sites 1, 4, 11, and 8.

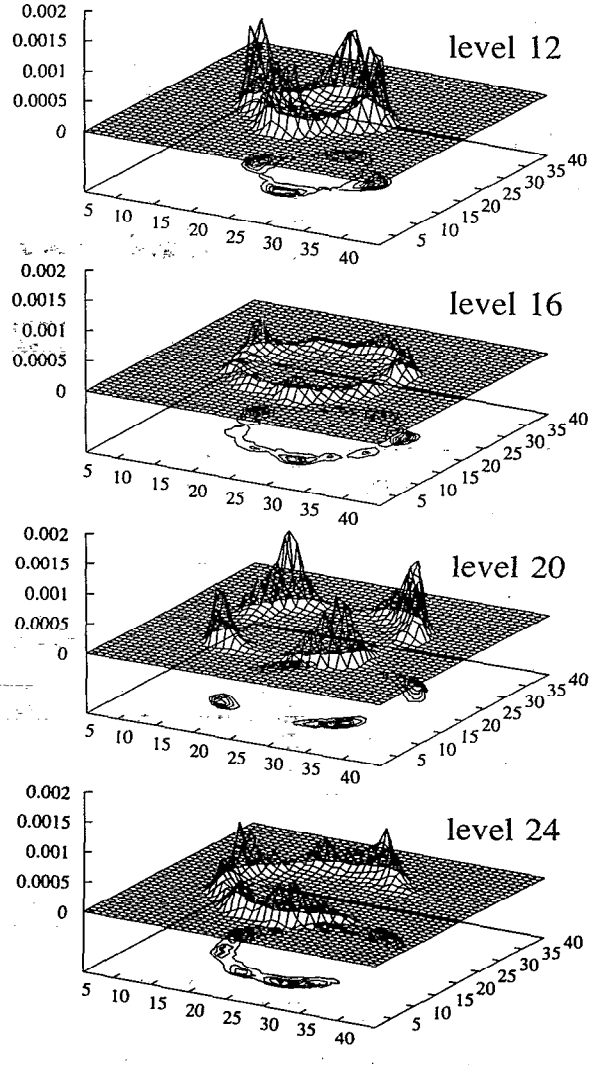

FIG. 4. Normalized one-body distribution function for a single Xe atom in the alpha cage at 300 K. The slices at levels 12, 16, 20, and 24 of the 40×40×40 stored distributions correspond to planes (a) through (d), respectively, in Fig. 2.

low-energy transition states that we found by using the method of Cerjan and Miller.[34] From the energies of the transition states displayed in Table I we see that activation energies for these low-energy paths are in the range 1200 to 3800 J/mol. Of these transition states, there are six that have higher energies than the others (3837–4018 J/mol relative to the lowest-energy adsorption site). Each of them is close to one of the six $Na(II)^+$ ions that are located off-center in the windows of the alpha cage. Other paths connecting adsorption sites involve going over much higher terrain. To illustrate, sites 1, 4, 8, and 11 are, respectively, at $x=6.1557$, 6.1490, 6.145, and 6.1498 Å, i.e., these sites are at the $x=6.15$ Å level. The potential energy surface at the $x=6.15$ Å slice is shown at the bottom of Fig. 3, to be compared with the $x=3.6$ Å plane, wherein lie sites 3, 5, 10, and 9 (top of Fig. 3). The latter are connected by low-energy paths whereas sites 1, 4, 8, and 11 are not. Because of the symmetry of the alpha cage, the $z=3.6$ Å plane contains sites 4, 5, 11, and 6 which are interconnected by low-energy paths. Similarly the $y=8.66$ Å plane contains sites 7, 8, 10, and 11, and the $y=3.6$ Å plane contains sites 1, 2, 4, and 3, likewise connected by low-energy paths, and so on. Thus, it might be expected that although sites 4 and 11 are only 5.06 Å apart, it is energetically more favorable for the Xe to go indirectly via 4–6–11 or 4–5–11. For comparison with the transition state energies shown in Table I, the potential energy of a Xe atom at the center of the alpha cage is 13 855 J/mol relative to the lowest-energy adsorption site.

B. One-body distribution functions

The information was collected by dividing the unit cell into 80×80×80 voxels and counting how many configurations placed the center of a xenon atom in each voxel. The symmetry permits the storing of the distribution in all eight alpha cages in one 40×40×40 array. The average one-body distribution is obtained for a given chemical potential and temperature, for which the simulation also provides the average occupancy per alpha cage, $\langle n \rangle$. But more interesting are the one-body distribution functions of the individual clusters, collected in the voxels from several runs at the same temperature. The normalized one-body distribution function obtained from simulations at 300 K provides the probabilities of finding the single atom in various locations in the alpha cage at this temperature. In Fig. 4 we show isometric

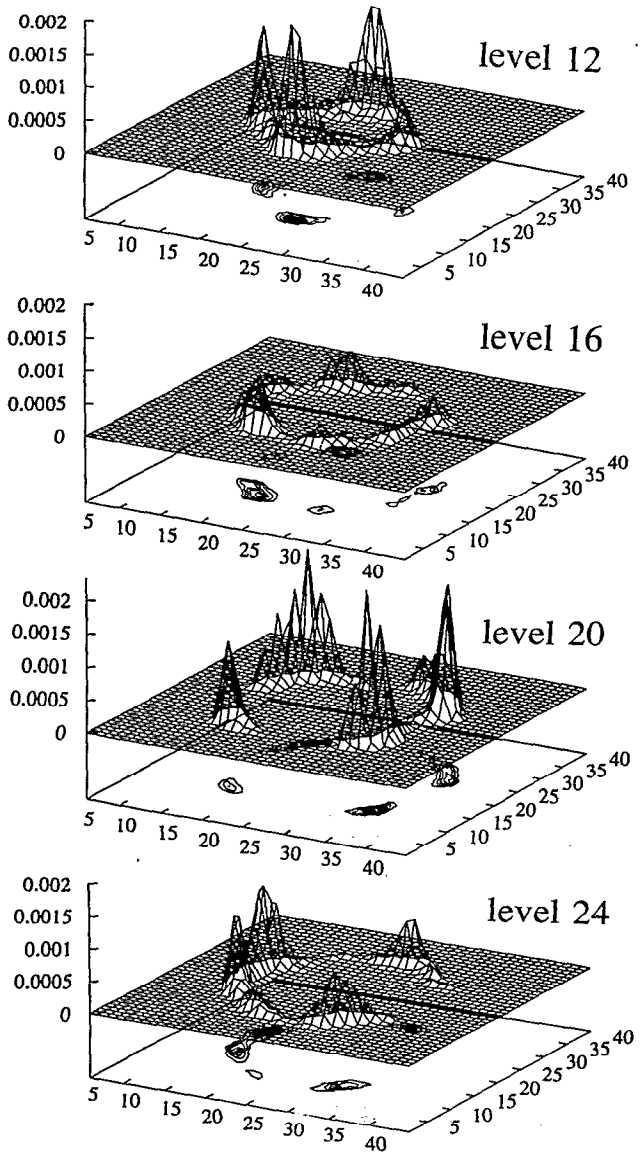

FIG. 5. Normalized one-body distribution function for a Xe_8 cluster in an alpha cage of zeolite NaA at 300 K in the same planes as Fig. 4.

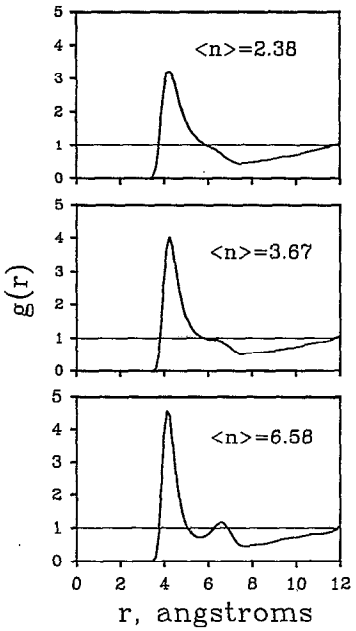

FIG. 6. Pair distribution functions for xenon in zeolite NaA at 220 K, normalized to the ideal gas distribution function.

and contour plots of the normalized probabilities for a single Xe atom in the alpha cage at 220 K at various levels. The normalized probability distribution for Xe_8 is shown in Fig. 5. Levels 12, 16, 20, and 24 of the 40×40×40 array of the stored one-body distribution corresponds to the planes selected to display the potential energy surface in Fig. 2, except that while Fig. 2 gives the potential energy at the designated z values, Figs. 4 and 5 provides an average one-body distribution for all points collected within each voxel whose centers are at these z values. A voxel is a cube which is 0.306 94 Å on a side. The type III Na^+ ion intrudes into the alpha cage, and introduces an asymmetry which is visible in the level 24 plot. In the comparison of the one-body distributions of Xe_8 with Xe_1, the very interesting feature is that the maxima are roughly in the same locations but Xe atoms in Xe_8 have more peaked distributions, i.e., there is a much smaller probability of being found in the regions between maxima in Xe_8. The second important feature to note is that the probability of an Xe atom being found in the middle of the alpha cage is very small, even in Xe_8. The physical picture that emerges is that the Xe atoms stay close to the walls of the cage whether there are one or two or even eight atoms in the cage. Only the one-body distributions for Xe_1 and Xe_8 are given here. The Xe_2 through Xe_7 one-body distributions do not offer any different physical insight. At a higher temperature the distribution is more spread out, but even so, at 360 K there is still a very small probability of finding a Xe atom in the middle region of the alpha cage. This is in agreement with other simulations of xenon in zeolites, the prominent feature in the one-particle distribution function is the maximum located close to the wall in every case, with the central regions of the cavities remaining unpopulated except at very high temperatures.[1,2,8,9]

C. The pair distribution functions

The pair distribution function provides additional details. The pair distribution function is the number of atoms at a distance r from a given atom compared with the number at the same distance in an ideal gas at the same density. Normalization is carried out as described by Allen and Tildesley.[35] The average $g(r)$ for a given loading can be obtained from any GCMC run and a few examples at 220 K are shown in Fig. 6. We note that a prominent feature of the pair distribution functions is the peak at around 4.2 Å. As expected, the sharp features become less so at higher temperatures (not shown). The high loading example in Fig. 6 exhibits a second peak. A better understanding of the average $g(r)$ can be gleaned from the $g(r)$ for each cluster which we also obtain. In Fig. 7 are the $g(r)$ for the Xe_n in the zeolite at 220 K. Xe_1, of course, shows only the neighboring cage contributions. Xe_2 shows that even when there are only two

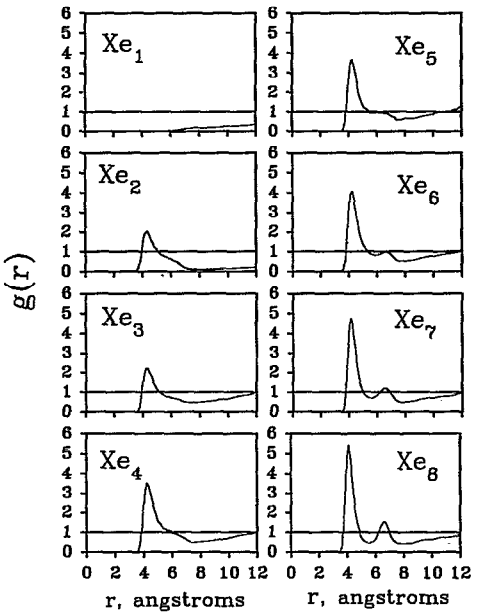

FIG. 7. Pair distribution functions at 220 K for Xe_n clusters in an alpha cage of zeolite NaA, normalized to the ideal gas distribution function. Xe_1 and Xe_2 were obtained from a simulation with $\langle n\rangle = 0.36$. Xe_3 and Xe_4 were obtained from a simulation with $\langle n\rangle = 3.66$, and Xe_5, Xe_6, Xe_7, and Xe_8 from a simulation with $\langle n\rangle = 6.58$.

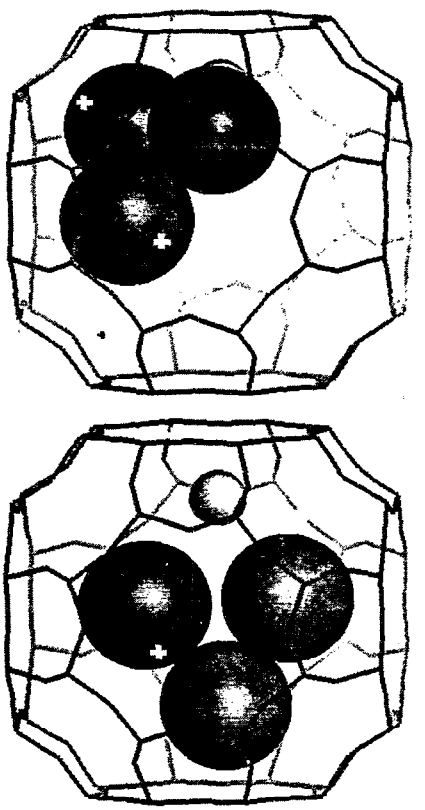

FIG. 8. Two of the minimum energy configurations for Xe_3. In the bottom figure (the global minimum energy configuration), the Xe atoms are close to sites 1, 8, and 9 (of Fig. 1) while in the top figure the Xe atoms are close to sites 2, 6, and 4.

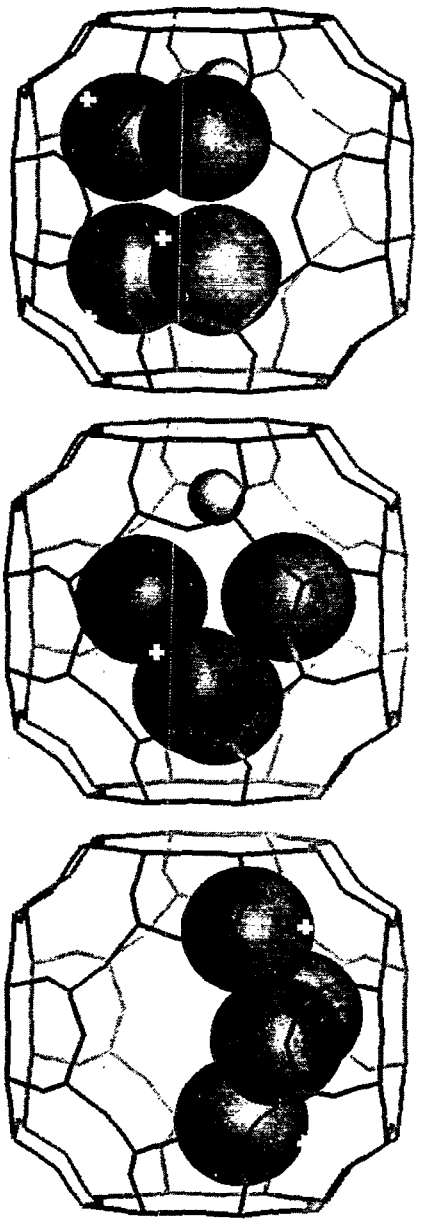

FIG. 9. Some minimum energy configurations for Xe_4. These are local minima in the configuration space of four Xe atoms in an alpha cage of zeolite NaA. In the top figure (the lowest-energy configuration) the atoms are close to sites 2, 3, 5, and 6.

Xe atoms in the cage, they are quite frequently found at the favorable Xe–Xe interaction distance of 4.2 Å (the $r_{\min}$ of the gas phase Xe_2 potential is at 4.3627 Å). In the pair distribution functions in Fig. 7, we will later be able to identify the second peak as one corresponding to the next-nearest site. This peak rises more sharply in going from Xe_6 to Xe_8. The average $g(r)$ that one gets for a given $\langle n\rangle$ will merely reflect these cluster $g(r)$ functions weighted according to the fractions of cages having such clusters $[f(n)]$.

D. The minimum energy configurations of the clusters Xe_2 through Xe_8

Starting points for the determination of the minimum energy configurations can be collected during the GCMC

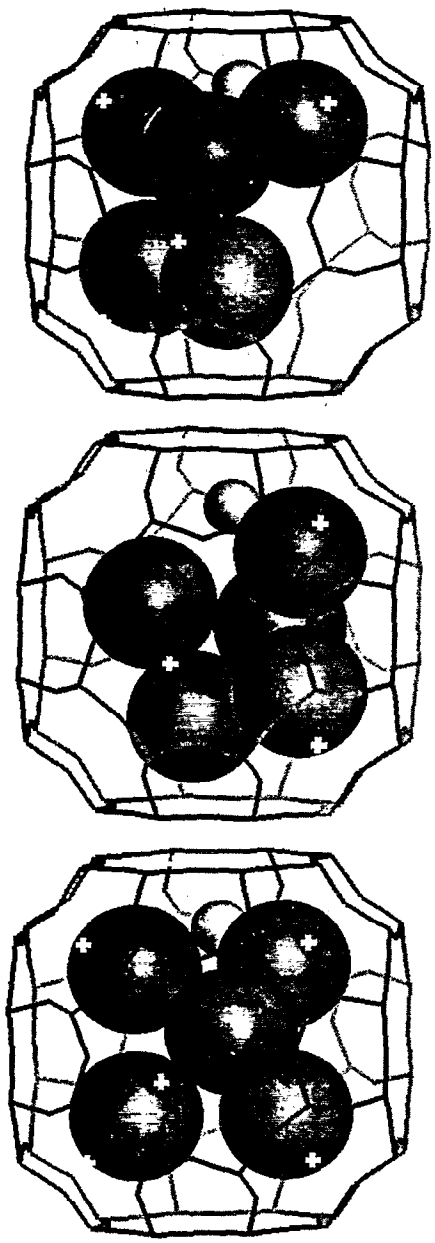

FIG. 10. Some minimum energy configurations for Xe_5. These are local minima in the configuration space of five Xe atoms in an alpha cage of zeolite NaA. In the top figure (the lowest-energy configuration) the Xe atoms are close to sites 2, 3, 5, 6, and 7.

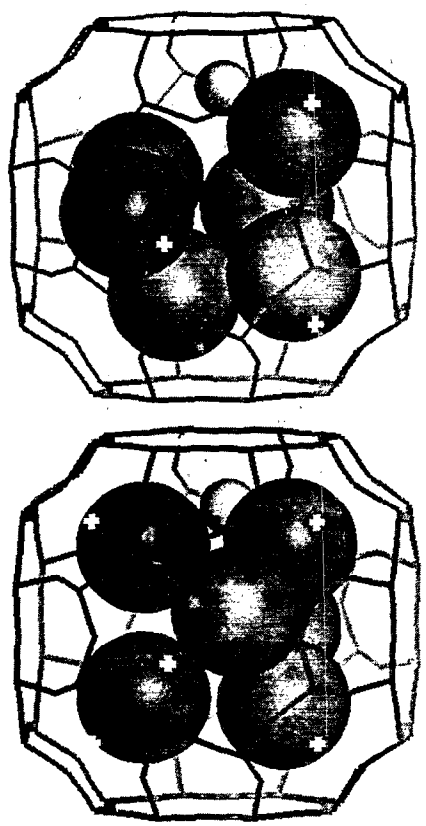

FIG. 11. Some minimum energy configurations for Xe_6. These are local minima in the configuration space of six Xe atoms in an alpha cage of zeolite NaA. The top figure is the minimum energy configuration, in which the Xe atoms are close to sites 1, 3, 4, 7, 8, and 10.

runs. One merely saves the lowest-energy configuration of each cluster found in the eight cages of the simulation box in each run. This automatically provides eight low-energy configurations for each cluster. First, the nondistinct configurations are eliminated by superposition of closest atoms and use of a greater-than-a-minimum distance criterion. The remaining low-energy configurations provide independent starting configurations each of which is close to a local minimum in the configuration space of that cluster, from which starting point any one of a number of methods of finding the local minimum can be used. When two or more presumed distinct low-energy configurations converge to the same local minimum in configuration space of that cluster, only one is retained. This way we have been able to find several local minima: distinct low-energy configurations for each cluster. In this process, we also found the same 11 configurations for the "Xe_1 cluster" as the 11 lowest-energy sites in the potential energy surface, of course. We converged to 14–25 distinct configurations each for Xe_2 through Xe_7, and six distinct configurations for Xe_8. A select number of these are shown in Figs. 8–13 for Xe_3 through Xe_8. A very interesting result is that the Xe_8 minimum energy configurations are "hollow" shells, i.e., there is no atom in the center of the alpha cage. Table III provides a survey of the distinct low-energy configurations found for Xe_2 through Xe_8. Each of these is a converged local minimum in the configuration space of each Xe_n and the energy quoted is relative to the global minimum for the Xe_n in the alpha cage. Some very interesting features of these minimum energy configurations are the following. First of all, they are not the same minimum energy configurations that are typically found for isolated rare gas clusters. Clusters of rare gas atoms tend to adopt deltahedral geometries wherein all the faces are triangular.[36] Second, some of the unique minimum energy configurations have the same cluster geometry. That is, two or more configurations that are unique in their geometry and orientation within the alpha cage are found to have very similar sets of Xe–Xe distances. For example, although we found 14 distinct local minima in the configuration space of

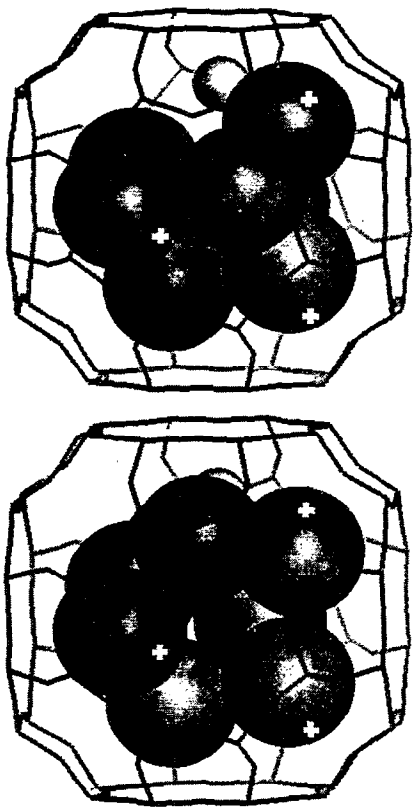

FIG. 12. Some minimum energy configurations for Xe_7. These are local minima in the configuration space of seven Xe atoms in an alpha cage of zeolite NaA. The top figure is the minimum energy configuration.

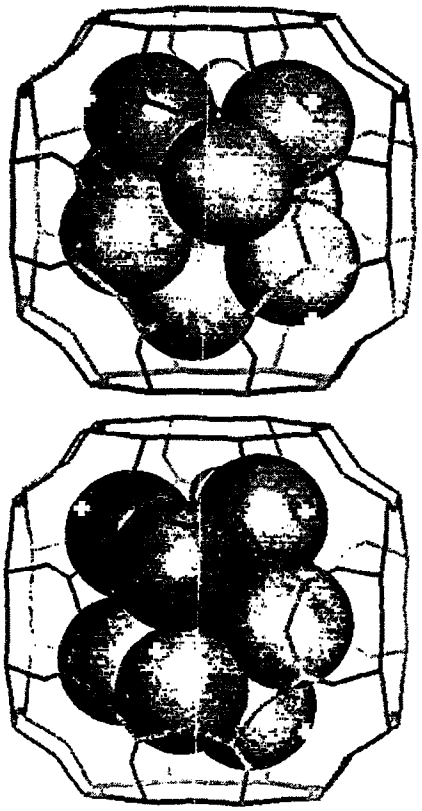

FIG. 13. Some minimum energy configurations for Xe_8. These are local minima in the configuration space of eight Xe atoms in an alpha cage of zeolite NaA. The top figure is the minimum energy configuration.

Xe_3 in the alpha cage, there are only three distinct geometries among the 14 configurations, as characterized by the complete set of Xe–Xe distances. Geometries were considered distinct if the Xe–Xe distances differ by more than 0.5 Å. Similarly, for Xe_4 in the alpha cage there are eight distinct geometries among the 14 minimum energy configurations. For Xe_6 there are 11 out of 17; for Xe_7 there are four distinct geometries out of 17; and for Xe_8 there are three distinct geometries out of six. Third, the Xe "layer" being incommensurate with the adsorption site locations, the Xe_n geometries are not simple extensions of the Xe_{n-1} geometries. The saddle points on the potential energy surface of Xe_n inside the alpha cage can be found by the Cerjan–Miller method, as has been previously demonstrated by Wales for isolated Ar_n clusters,[37] or by the slowest slides algorithm proposed by Berry *et al.*[38] A systematic search for transition states of a particular Xe_n cluster in an alpha cage has not yet been carried out. Lower-lying saddles connecting the most stable local minima in the configuration space would provide activation energies for rearrangement of the clusters. Interpretation of the variable temperature studies of the ^{129}Xe NMR relaxation of the clusters at very low temperatures may require this type of information.

Let us now consider the distributions of Xe–Xe distances found in the configurations which correspond to local minima in the configuration space of a cluster. The distances between the 11 adsorption sites for a single Xe atom in the alpha cage of zeolite NaA are 3.6, 5.1, 6.2, and 7.2 Å. The 14 local minima we found in the Xe_2 configuration space have Xe–Xe distances which are either 4.2 or 4.7 Å. It is energetically unfavorable for two Xe atoms to be in register with the Xe–zeolite potential minima and simultaneously be 3.6 Å apart. The large Xe–Xe repulsive interaction at such close separations is relieved by a compromise arrangement in which the Xe–Xe distance is near the $r_{\min}$ of the Xe_2 potential while each Xe is still within an rms distance of 0.2 Å from its corresponding adsorption site. The second peak in the Xe–Xe distances for Xe_2 in the cage is 4.7 Å, whereas next-nearest-neighbor adsorption sites are 5.1 Å apart. This appears to be a compromise of two Xe atoms in two sites 5.1 Å apart being attracted to each other such that the lowest-energy configurations correspond to Xe–Xe separations somewhat closer than the site-to-site distance. Examination of Xe_3 reveals similar compromises. The 14 Xe_3 clusters we found have Xe–Xe distances of 4.2 (most common), 4.5, 4.7, and 6.2 Å, demonstrating sorbate–sorbate interactions have an important role to play in the "occupancy" of adsorption sites. The distributions of Xe–Xe distances for the minimum energy configurations that we found are shown in Fig. 14 although these are only some of the large number of possible configurations which are local minima in the cluster configuration space. The features that are seen in the $g(r)$ function for the Xe_n clusters from the GCMC simulations at 220 K in Fig. 7 can be observed in Fig. 14 and identified with the most

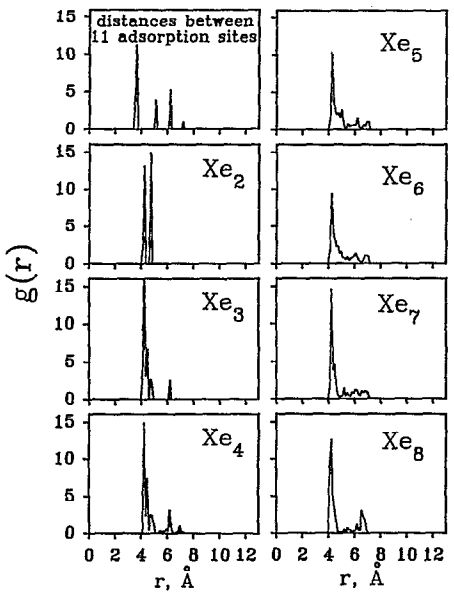

FIG. 14. The distribution of distances between adsorption sites for a single Xe atom in the alpha cage of zeolite NaA and the distributions of Xe–Xe distances in the minimum energy configurations of clusters of Xe_2 through Xe_8. The number of configurations that correspond to local minima in the configuration space of Xe_n which have been found, on which the above distribution of distances is based, are 18, 14, 14, 25, 17, 17, and 6, respectively, for Xe_2 through Xe_8.

commonly found internuclear distances in the various minimum energy configurations of Xe_n clusters. The sharpening up of the peak at 6.6 Å in Fig. 7 can be understood by comparison with Fig. 14. The crowded cage with Xe_8 limits the number of favorable compromises in Xe–Xe and Xe-adsorption site distances.

The Xe atoms in a cluster Xe_n are found close to the minimum energy sites for the single Xe atom (adsorption sites). The similarity of the one-body distribution function for Xe_8 in Fig. 5 to the one-body distribution function for a single Xe in the alpha cage in Fig. 4 needs some explanation. We find that the individual coordinates for the Xe atoms in the local minima we found in the configuration space of the clusters Xe_2 through Xe_8 are all somewhat close to the coordinates of the 11 adsorption sites. The closest distances of the Xe atoms in a cluster from the 11 Xe adsorption sites of a single Xe atom in an alpha cage are shown in Table II as rms distances. In general, the rms distances become larger with a larger number of Xe atoms in the cage, but even for eight Xe atoms, each one is no further than 1.0–1.2 Å away from its corresponding adsorption site.

E. Do ordered structures exist for Xe in the alpha cage?

It has been suggested in several papers[20–23] that xenon atoms (Kr and Ar as well)[24] form highly ordered structures in the cavities at high loadings. Molecular dynamics (MD) simulations yield ordered structures for all the rare gases in zeolite rho at high loadings, and the ordering is not particularly sensitive to temperature.[23,24] For example, Xe is found in MD simulations to form a nine-atom/cage simple body-centered cubic array[23] whereas Kr forms a 15-atom distorted face-centered-cubic array with a central atom.[24] The trajectories in the MD simulations become very localized at these loadings. It has been suggested that these structures are produced by packing requirements for the sorbate atoms in a rigid cage rather than their attractive interactions. The one-body distribution functions that we find for Xe_8 in the alpha cage of NaA do not correspond to a single ordered structure. The maxima in the distribution function are close to, although not exactly at, the locations of the maxima in the distribution function of Xe_1 in the GCMC simulations at temperatures in the range 200–360 K. We find therefore, that we do not have the highly localized ordered structures found by others. Rather, the various low-energy configurations that we have found for Xe_8, e.g., are configurations with the Xe atoms located close to (but not at) eight of the 11 adsorption sites (the minimum energy locations for Xe_1). The Xe_8 one-

TABLE II. The rms distances of the Xe atoms in a Xe_n cluster minimum energy configuration to the corresponding closest adsorption sites (Å).

	Configuration, arranged according to energy							
Cluster	1	2	3	4	5	6	7	8
Xe_2	0.204	0.196	0.248	0.243	0.211	0.200	0.212	0.201
Xe_3	0.878	0.717	0.446	0.439	0.896	0.760	0.477	0.478
Xe_4	0.473	0.476	0.478	0.511	0.429	0.560	1.141	0.940
Xe_5	0.546	0.984	0.569	0.530	1.028	0.977	0.511	0.817
Xe_6	0.934	1.014	0.929	0.974	0.766	0.782	0.750	0.642
Xe_7	1.020	0.892	0.894	0.854	1.053	0.814	0.940	0.880
Xe_8	1.171	1.144	1.131	1.073	1.124	1.064		
Cluster	9	10	11	12	13	14	15	16
Xe_2	0.364	0.361	0.354	0.355	0.245	0.241	0.429	0.393
Xe_3	0.448	0.714	1.016	0.401	0.372	0.413		
Xe_4	0.944	0.864	0.855	0.675	0.469	0.455		
Xe_5	0.811	0.595	0.613	1.085	0.577	0.855	0.919	0.977
Xe_6	0.848	0.717	0.815	0.593	0.870	0.818	0.593	0.870
Xe_7	0.864	0.956	1.129	1.038	0.922	1.074	0.776	0.993

TABLE III. A survey of the relative energies of the local minimum configurations of the clusters in J/mol. (These are only some of the local minima found in the configuration space of Xe_n in the alpha cage.)

	Configuration number							
Cluster	1	2	3	4	5	6	7	8
Xe_2	0.0	39.9	68.6	120.3	157.1	206.7	211.0	260.2
Xe_3	0.0	123.1	163.8	166.6	332.3	422.5	442.6	443.0
Xe_4	0.0	1.9	264.7	312.9	336.5	604.7	965.8	969.4
Xe_5	0.0	33.3	301.0	499.0	569.2	629.5	650.5	804.4
Xe_6	0.0	208.5	515.7	699.5	706.0	757.2	861.1	1007.3
Xe_7	0.0	148.4	151.8	313.8	530.5	581.3	654.1	721.9
Xe_8	0.0	23.6	1497.1	1652.3	1686.4	3074.7		
Cluster	9	10	11	12	13	14	15	16
Xe_2	305.4	307.0	387.4	403.5	405.4	448.2	466.8	451.9
Xe_3	490.5	508.1	700.3	729.2	741.6	806.9		
Xe_4	977.7	1268.3	1306.5	1404.3	1700.7	1982.8		
Xe_5	809.2	910.7	965.3	1085.2	1085.8	1141.8	1324.2	1367.3
Xe_6	1027.3	1050.3	1098.9	1146.2	1153.6	1229.9	1291.9	1735.7
Xe_7	980.5	1138.3	1210.7	1321.1	1492.8	1650.2	1708.2	1797.3

body distribution function shows 11 peaks not eight, i.e., Fig. 5 shows that many of the low-energy configurations of Xe_8 are sampled, not only one. Therefore, at these temperatures, Xe_8 does not form an ordered structure. It may be that the ordered structures exist only for a very short period of time and that the duration of the MD simulations do not permit the exploration of other configurations. Furthermore, we do not find any of the ordered structures suggested by the canonical Monte Carlo simulations in model cavities.[20,21] Is the large incremental NMR shift between Xe_6 and Xe_7 (or Xe_7 and Xe_8) associated with particular cluster geometries, as suggested by these authors? In the preceding paper[25] the average ^{129}Xe shieldings for the Xe_n clusters at various temperatures were predicted very successfully by the GCMC simulations without invoking any preferred configurations. In Figs. 4, 5, and 7 the one-body and the pair distribution functions for the Xe in the alpha cage change in a systematic way in going from the Xe_1 to the Xe_8 cluster. There is no apparent discontinuity between the Xe_6 and Xe_7 distributions, so that a jump in the chemical shift cannot be attributed to the occurrence of any specific geometry change. Rather, the smooth precipitous drop in the ^{129}Xe shielding function at short range, accompanied by the prevalence of short distances in the overcrowded cage for the larger clusters result in the much larger increments in the chemical shifts for these larger clusters, especially at the higher temperatures which permit the enhanced sampling of the shorter Xe–Xe distances at which the ^{129}Xe shieldings are very paramagnetic.

III. CONCLUSIONS

The characteristics of the adsorbed fluid in the Xe in zeolite NaA system are provided by the GCMC simulations. Since these simulations gave quantitatively the same adsorption isotherm as has been found by experiment, the same fractions of alpha cages containing zero through eight Xe atoms as had been measured in all ten samples at both 296 and 360 K, and provided quantitative agreement with the observed absolute chemical shifts of the clusters and their temperature dependence in the range 188–420 K, then we have a reasonable expectation that the characterization of the structure of the adsorbed fluid in the GCMC simulations can provide some insight into the characteristics of the adsorbed fluid in the zeolite. We found 11 local minima for a single Xe atom in the alpha cage (adsorption sites). We have shown some of the minimum energy configurations that we have found for the clusters Xe_2 through Xe_8, the one-body distributions for Xe_1 and for Xe_8, and the pair distribution functions for the clusters Xe_2 through Xe_8. We relate these pair distribution functions to the distribution of distances between atoms in the local minima in the configuration space of the clusters Xe_2 through Xe_8. From the low-energy transition states that we have determined for the Xe–zeolite potential function used here we deduce that a single Xe atom has easy access to three or four sites via paths along the walls of the alpha cage. All indications are that at room temperature, the Xe atom is not found in the middle of the alpha cage, not when it is alone in the cage, not even when there are eight Xe atoms in the alpha cage. There appear to be several low-energy cluster configurations that are distinct from each other for each cluster size, and there are no particular cluster configurations or change of configurations that are specifically responsible for the large simulated and experimental incremental shift between Xe_6 and Xe_7 and between Xe_7 and Xe_8.

ACKNOWLEDGMENTS

This research has been supported by the National Science Foundation (Grant No. CHE92-10790). C.J.J. thanks Professor John Rowlinson for providing the opportunity to learn about GCMC simulations in the Physical Chemistry Laboratory, Oxford University, and Michael Maddox for help during the learning process. Figures 8–12 were drawn using the program MOILVIEW (Carlos Simmerling, UIC).

[1] G. B. Woods, A. Z. Panagiotopoulos, and J. S. Rowlinson, Mol. Phys. **63**, 49 (1988).
[2] G. B. Woods and J. S. Rowlinson, J. Chem. Soc. Faraday Trans. 2 **85**, 765 (1989).
[3] J. L. Soto and A. L. Myers, Mol. Phys. **42**, 971 (1981).
[4] E. Cohen de Lara and J. Vincent-Geisse, J. Phys. Chem. **80**, 1922 (1976).
[5] E. Cohen de Lara, R. Kahn, and A. M. Goulay, J. Chem. Phys. **90**, 7482 (1989).
[6] S. Yashonath, J. M. Thomas, A. K. Nowak, and A. K. Cheetham, Nature **331**, 601 (1988).
[7] S. Yashonath, P. Demontis, and M. L. Klein, Chem. Phys. Lett. **153**, 551 (1988).
[8] S. Yashonath, Chem. Phys. Lett. **177**, 54 (1991); J. Phys. Chem. **95**, 5877 (1991).
[9] S. Yashonath and P. Santikary, Phys. Rev. B **45**, 1095 (1992).
[10] P. Santikary and S. Yashonath, J. Chem. Soc. Faraday Trans. **88**, 1063 (1992).
[11] B. Smit and C. J. J. den Ouden, J. Phys. Chem. **92**, 7169 (1988).
[12] S. D. Pickett, A. K. Nowak, J. M. Thomas, B. K. Peterson, J. E. P. Swift, A. K. Cheetham, C. J. J. den Ouden, B. Smit, and M. F. M. Post, J. Phys. Chem. **94**, 1233 (1990).
[13] A. K. Nowak, A. K. Cheetham, S. D. Pickett, and S. Ramdas, Mol. Simul. **1**, 67 (1987).
[14] S. Fritzche, R. Haberlandt, J. Kaerger, H. Pfeifer, and M. Wolfsberg, Chem. Phys. Lett. **171**, 109 (1990).
[15] R. L. June, A. T. Bell, and D. N. Theodorou, J. Phys. Chem. **94**, 1508, 8232 (1990); **95**, 8866 (1991); **96**, 1051 (1992).
[16] R. Q. Snurr, R. L. June, A. T. Bell, and D. N. Theodorou, Mol. Simulations **8**, 73 (1991).
[17] J. M. D. MacElroy and K. Raghavan, J. Chem. Soc. Faraday Trans. **87**, 1971 (1991).
[18] J. M. D. MacElroy and K. Raghavan, J. Chem. Phys. **93**, 2068 (1990).
[19] P. Demontis, E. S. Fois, G. B. Suffritti, and S. Quarteri, J. Phys. Chem. **94**, 4329 (1990).
[20] P. R. van Tassel, H. T. Davis, and A. V. McCormick, Mol. Phys. **73**, 1107 (1991).
[21] P. R. van Tassel, H. T. Davis, and A. V. McCormick, Mol. Phys. **76**, 411 (1992).
[22] P. R. van Tassel, H. T. Davis, and A. V. McCormick, J. Chem. Phys. **98**, 8919 (1993).
[23] A. V. Vernov, W. A. Steele, and L. Abrams, J. Phys. Chem. **97**, 7660 (1993).
[24] A. Loriso, M. J. Bojan, A. Vernov, and W. A. Steele, J. Phys. Chem. **97**, 7665 (1993).
[25] C. J. Jameson, A. K. Jameson, B. I. Baello, and H. M. Lim, J. Chem. Phys. **100**, 5965 (1994).
[26] A. K. Jameson, C. J. Jameson, and H. S. Gutowsky, J. Chem. Phys. **53**, 2310 (1970).
[27] J. J. Pluth and J. V. Smith, J. Am. Chem. Soc. **102**, 4704 (1980).
[28] J. M. Bennett, C. S. Blackwell, and D. E. Cox, in *Intrazeolite Chemistry*, edited by G. D. Stucky and F. G. Dwyer, ACS Symp. Series 218 (Ameri-

can Chemical Society, Washington, D.C., 1983), p. 143.
[29]G. B. Woods, D.Phil. thesis, Oxford University (1989).
[30]G. C. Maitland, M. Rigby, E. B. Smith, and W. A. Wakeham, *Intermolecular Forces, their Origin and Determination* (Clarendon, Oxford, 1981).
[31]R. A. Aziz and M. J. Slaman, Mol. Phys. **57**, 825 (1986).
[32]C. J. Jameson and A. C. de Dios, J. Chem. Phys. **97**, 417 (1992); **98**, 2208 (1993).
[33]G. E. Norman and V. S. Filinov, High Temp. USSR **7**, 216 (1969).
[34]C. J. Cerjan and W. H. Miller, J. Chem. Phys. **75**, 2800 (1981).
[35]M. P. Allen and D. J. Tildesley, *Computer Simulation of Liquids* (Clarendon, Oxford, 1987).
[36]M. R. Hoare and P. Pal, Adv. Phys. **20**, 161 (1971); M. R. Hoare, Adv. Chem. Phys. **40**, 49 (1979).
[37]D. J. Wales, J. Chem. Phys. **91**, 7002 (1989).
[38]R. S. Berry, H. L. Davis, and T. L. Beck, Chem. Phys. Lett. **147**, 13 (1988).